Analyzing powers of inelastic *dp* scattering in the energy region of Δ and Roper resonances excitation

L. V. Malinina,[1] G. D. Alkhazov,[2] W. Augustyniak,[3] M. Boivin,[4] J.-L. Boyard,[5] R. Dahl,[6] M. Drews,[6] C. Ellegaard,[6] L. Fahri,[5] C. Gaarde,[6,†] T. Hennino,[4,5] J. C. Jourdain,[5] M. Kagarlis,[4] A. V. Kravtsov,[2] R. Kunne,[4,5] J. S. Larsen,[6] P. Morsch,[7] V. A. Mylnikov,[2] E. M. Orischin,[2] C. F. Perdrisat,[8] N. M. Piskunov,[1] A. N. Prokofiev,[2] V. Punjabi,[9] P. Radvanyi,[4,5] B. Ramstein,[5] B. V. Razmyslovich,[2] M. Roy-Stephan,[5] I. M. Sitnik,[1] M. Skousen,[6] E. A. Strokovsky,[1] I. I. Tkach,[2] E. Tomasi-Gustafsson,[4,10] S. S. Volkov,[2] A. A. Zhdanov,[2] and P. Zupranski[3]

[1]*JINR, RU-141980 Dubna, Moscow district, Russia*
[2]*PNPI, RU-188300 Gatchina, St. Petersburg district, Russia*
[3]*Andrzej Soltan Institute for Nuclear Studies, Warsaw, Poland*
[4]*LNS, CEA/DSM, and CNRS/IN2P3, CE Saclay, F-91191 Gif sur Yvette Cedex, France*
[5]*IPN CNRS/IN2P3 and Université Paris-sud, F-91400 Orsay, France*
[6]*Niels Bohr Institutet, Copenhagen, Denmark*
[7]*KFZ-Juelich, D-52425 Juelich, Germany*
[8]*The College of William and Mary, Williamsburg, Virginia 23185*
[9]*Norfolk State University, Norfolk, Virginia 23504*
[10]*CEA/DAPNIA/SPhN, CE Saclay, F-91191 Gif sur Yvette Cedex, France*

(Received 6 March 2001; published 21 November 2001)

A study of inelastic scattering of polarized 3.73-GeV/c deuterons on protons in the energy region of the Roper $N(1440)$ and the $\Delta(1232)$ resonances excitation has been performed in an exclusive experiment at LNS (Laboratoire National SATURNE, Saclay, France) using the SPES4-π setup. Tensor and vector analyzing powers of pion production for the reactions: $d+p\rightarrow d+n+\pi^+$, $d+p\rightarrow d+p+\pi^0$, $d+p\rightarrow d+N+\pi\pi$ have been measured as functions of the squared deuteron four-momentum transfer t, of the effective mass of the subsystems $N\pi$, $N\pi\pi$, and of the pion emission angle. A strong dependence of these analyzing powers upon the pion emission angle is observed. It is found that A_{yy} values for the considered reaction channels are systematically larger than the known inclusive $p(d,d')X$ world data at the nearest beam energy.

DOI: 10.1103/PhysRevC.64.064001 PACS number(s): 13.88.+e, 13.75.−n, 24.30.Gd, 25.45.−z

I. INTRODUCTION

The excitation of broad hadronic resonances in nuclei by isoscalar projectiles has been studied intensively in recent years [1–5]. The inelastic interaction of isoscalar projectiles (as α or d) with a proton holds the prospect of isolating isobar excitations according to their isospin. The simplest process is the one where the target is excited to an isobar that then must have $I=1/2$. It must occur through isoscalar meson exchange. There is also a possibility that the excitation occurs in the projectile through exchange of an isoscalar or an isovector meson, in the latter case the Δ can also contribute (Fig. 1).

The interest of a study of the $N^*(1440)$ (the Roper resonance) excitation by isoscalar projectiles was revived several years ago, following the observation of isospin-1/2 excitation of the proton in the region of the Roper resonance $N^*(1440)$ in the inclusive $p(\alpha,\alpha')X$ [4] and $p(d,d')X$ reactions [5]. The contribution to the total cross section of inelastic (α,α') and (d,d') scattering from the amplitude corresponding to Δ excitation is large at energies of several GeV. Therefore, the analysis of these processes in terms of the Roper resonance excitation is not free from ambiguities. The deuterons, conserving all advantages of an isoscalar projectile, is a spin-1 particle; therefore, using a polarized deuteron beam one can study polarization effects and obtain new information about the excitation of hadronic resonances.

The simplest polarization observable for $p(d,d')X$ is the tensor analyzing power A_{yy}. It was measured inclusively in Dubna and Saclay in 1993 and 1994 [6,7]. The experimental data show that it increases with increasing of $|t|$ almost linearly up to $|t|\simeq 0.3$ $(\mathrm{GeV}/c)^2$ and decreases at higher $|t|$. Such a behavior of the tensor analyzing power is fairly well reproduced in the theoretical framework of the exchange of ω meson in an algebraic collective model used for the electroexcitation of nucleon resonances [8,9]. In that approach

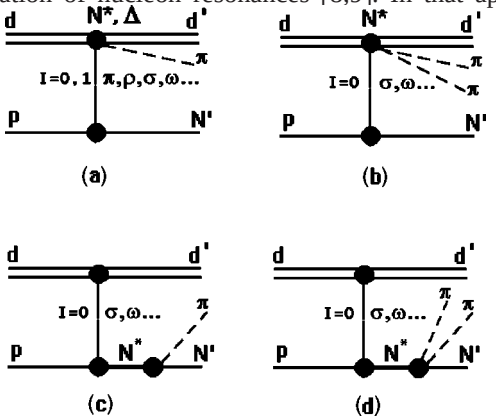

FIG. 1. Basic diagrams contributing to $p(d,d')N\pi(\pi)$ reaction: (a) One-pion production via Δ or N^* resonance excitation "in the deuteron." (b) Two-pion production via Roper excitation in the deuteron. (c),(d) One- and two-pion production via Roper excitation in the target.

†Deceased.

TABLE I. Experimental and setup parameters.

Forward Spectrometer	
Coordinate resolution σ	$\sim$0.3 mm
Momentum resolution $\delta p/p$	$\sim$5%
Horizontal angular resolution $\delta\theta_x$	$\sim$0.02 rad
Vertical angular resolution $\delta\theta_y$	$\sim$0.0014 rad
SPES4	
Momentum resolution $\delta p/p$	0.4%
Angular acceptance	3×10^{-4} sr
Momentum acceptance $\Delta p/p$	$\pm$4%
Horizontal angular acceptance $\Delta\theta_x$	(−0.0135, 0.0185) rad
Vertical angular acceptance $\Delta\theta_y$	$\pm$0.0114 rad
Beam and experimental parameters	
Trigger	SPES4 (FS + LS)
Missing mass resolution in the nucleon mass region	$\sim$20 MeV/c^2
Full/empty target ratio for selected events	$\sim$20
Deuteron beam momentum	3.73 GeV/c
Average beam polarization P_{ZZ}	0.902$\pm$0.015
Average beam polarization P_Z	0.311$\pm$0.008
Beam polarization control	Low-energy polarimeter $d(d,p)t$, E_d=400 KeV
Average beam intensity	$\sim10^6$/spill
Liquid hydrogen target dimensions	Length 6 cm; diameter 3 cm

the tensor analyzing power is expected to be very sensitive to the isoscalar longitudinal form factor of the Roper resonance excitation, while the other low mass nucleon resonances $S_{11}(1535)$, $D_{13}(1520)$, and $S_{11}(1650)$ have only isovector longitudinal form factors [9]. This specific property of the Roper resonance combined with the t dependence of the deuteron form factors determines the t behavior of the tensor analyzing power A_{yy}. An attempt to analyze the experimental data for the inclusive $p(d,d')X$ reaction in the framework of this model has been done in [10].

A guiding idea of the present experiment was that by comparing the single and double pion final states, one could distinguish the two reaction channels further. Selection of two-pion events would have the effect of eliminating $I=3/2$ projectile excitation contributions.

In this paper, we present data for the tensor and vector analyzing powers in dp inelastic scattering at kinetic energy $T_d=2430$ MeV, which is very close to the $N^*(1440)$ excitation threshold [$\sim$30 MeV in the nucleon-nucleon (NN) center-of-mass system (c.m.s.)].[1] The scattered deuterons were registered at angles close to 0.4° (Table I). The kinematics of $dp\rightarrow d'X$ reaction was almost collinear. The present exclusive experiment was performed at the SATURNE-II accelerator with the SPES4-π setup. The experimental data contain information about the following channels of the inelastic deuteron scattering on protons:

$$dp\rightarrow dp\pi^0, \tag{1}$$

$$dp\rightarrow dn\pi^+, \tag{2}$$

$$dp\rightarrow dN\pi\pi. \tag{3}$$

The channels with one pion in the final state can occur both from the Δ and N^* resonance decays

$$d+p\rightarrow d+N^*(1440), \qquad N^*\rightarrow p+\pi^0, \tag{4a}$$

$$d+p\rightarrow d+N^*(1440), \qquad N^*\rightarrow n+\pi^+, \tag{4b}$$

$$d+p\rightarrow d^*+p, \qquad d^*\rightarrow d+\pi^0, \tag{5}$$

$$d+p\rightarrow d^*+n, \qquad d^*\rightarrow d+\pi^+, \tag{6}$$

where d^* is the scattered deuteron with one of its nucleons excited in the Δ state. In the region of the resonance overlapping, an interference between the decay of the Δ and N^* may take place.

The tensor and vector analyzing powers for different channels of (d,d') reaction have been measured as functions of the squared deuteron four-momentum transfer t, or the effective mass of the binary subsystem $(N\pi)$ (see Fig. 2), and the pion emission angle in the reaction plane relative to incident deuteron momentum. The kinematical region for the

[1]Deuteron is a weakly bound state so mainly only one of its nucleons participates in the interaction. In pp ($p_p=p_d/2$) kinematics, $T_p=1215$ MeV: $T^{threshold}_{pp\rightarrow pN^*}=1138$ MeV. In dp, $T_d=2430$ MeV: $T^{threshold}_{dp\rightarrow dN^*}=1620$ MeV.

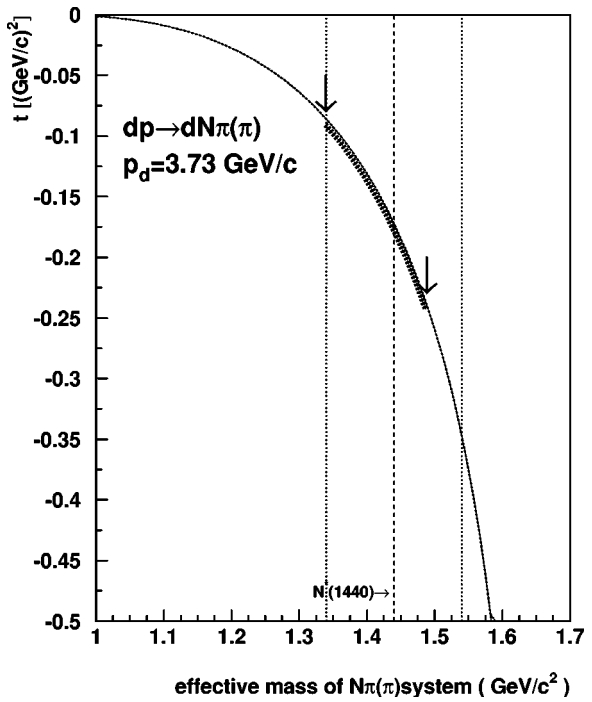

FIG. 2. Missing mass M_x [the effective mass $N\pi(\pi)$] versus four-momentum transfer $|t|$ at the deuteron beam momentum of 3.73 GeV/c. The dashed area represents the region covered in this experiment.

$d+p\rightarrow d+X$ reaction in the (t,M_X) plane studied in this experiment is shown in Fig. 2.

II. EXPERIMENTAL SETUP

The SPES4-π setup that was used in a series of experiments at SATURNE-II is shown in Fig. 3. It consists of a large acceptance nonfocusing magnetic spectrometer [magnet Tethys and detectors: forward spectrometer (FS) and lateral spectrometers (LS)] in combination with the high resolution focusing magnetic spectrometer SPES4 [11]. Below we shall confine our consideration to the forward spectrometer only (described in detail in [12]), since the LS information was not used in the present analysis. The particles of high momenta (in this experiment, scattered deuterons) were detected in SPES4 while the secondary low-momentum charged particles (protons and pions from the reactions listed above) were detected in the nonfocusing magnetic spectrometer FS.

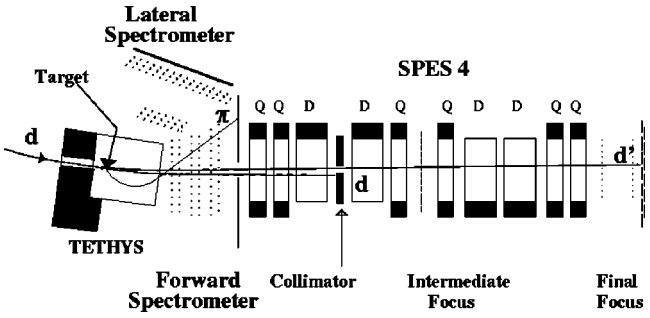

FIG. 3. SPES4-π setup.

A. SPES4

The SPES4 spectrometer is about 33 meters long and consists of four dipoles, six quadrupoles, and a correcting sextupole. Two scintillation hodoscopes I and F are located at the intermediate and the final foci, respectively. The hodoscope in the intermediate focus I consists of a row of scintillation counters while F consists of two rows of overlapping counters. The following combinations of the signals from scintillation counters were used for the trigger, SPES4$=(I_iF_i)+(I_iF_{i+1})$, where i is the counter number. Two 2-cm thick scintillators (ΔE detector) were placed after the hodoscope F to measure the detected particle ionization loss. Two drift chambers (with four wire planes each) placed before the F hodoscope served for the momentum reconstruction of scattered particle, however, in this experiment these chambers were not used and the deuteron momentum was reconstructed from the F-counter numbers. The resulting momentum resolution was $\simeq 0.4\%$ [13].

Particles were identified by time of flight and energy loss in the ΔE detector. This information was used to separate deuterons from background protons from the elastic $dp\rightarrow pd$ backward scattering.

The angular acceptance of the spectrometer was $\sim 3\times 10^{-4}$ sr.

In this experiment the outgoing beam was trapped after the first dipole of SPES4 by a 50-cm thick lead beam stopper. The directions of the outgoing beam and of the particle detected in SPES4 were separated less than 1° at the entrance of SPES4.

B. Tethys

The analyzing magnet Tethys was one of the two magnets that formed earlier the CERN split field magnet. Its horizontally oriented pole face has the shape of a square with a side of 100 cm, the pole aperture being 50 cm. The magnet was oriented with its iron yoke in the direction of the incoming beam. A hole of 20 cm width and 10 cm height provided a free path for the beam inside the magnet. Placed on air cushions, the magnet could be rotated around a fixed point, thus permitting the alignment of the entry hole with the direction of the incoming beam. The latter could be varied, thus allowing the selection of that part of the angular domain of the reaction that one wanted to study. A 6-cm long liquid hydrogen (LH) target was placed in the magnetic field approximately 25 cm after the entry hole.

The vertical component of the magnetic field was measured at three field strengths (0.6, 0.9, and 1.2 T), both in the median plane and in the plane 15 cm above the median plane. From the measured field values, a three-dimensional field map was constructed and extrapolated to a surface of 4×3.7 m^2 [14]. In this experiment three maximal values of the magnetic field were used: 0.7892, 0.8142, and 0.8418 T, corresponding to three central momenta of the SPES4 2.85, 2.94, and 3.04 GeV/c respectively.

C. The Forward Spectrometer

The FS consisted of six drift chambers $(X1,Y1,U,V,Y2,X2)$ and a scintillator hodoscope placed be-

TABLE II. Maximum values of the beam vector and tensor polarization parameters for the used beam polarization states at SATURNE-II (taken from [21]).

Number of the beam polarization state	P_{ZZ}^{max}	P_Z^{max}
5	+1	+1/3
6	+1	−1/3
7	−1	+1/3
8	−1	−1/3

hind the chambers. It was used for triggering and for particle identification. The $X1$ and $X2$ coordinates defined the intersections of the charged particle trajectory with the chamber planes in the horizontal direction, while the $Y1$ and $Y2$ coordinates in the vertical one; in addition U and V planes, with wires inclined by an angle of about $\pm 10°$ to the vertical axis, helped resolve many-particle ambiguities. The active area of the planes varied from 0.5×1.2 m^2 $(X1,Y1)$ to 0.7×1.7 m^2 $(X2,Y2)$. The scattered deuterons as well as the unscattered beam passed through a hole in each of the FS chambers and the FS hodoscope into the SPES4 entrance. The size of these holes was about 10×13 cm^2 in the chambers and 20×30 cm^2 in the hodoscope. Particles detected in the FS were identified by the time of flight and the energy loss in the hodoscope.

The procedure of alignment of the FS and the momentum reconstruction algorithm are described in [13,14].

D. The beam and monitors

The deuteron beam polarization was changed in the usual burst-to-burst mode; states 5, 6, 7, 8 (in SATURNE-II notations, see Table II), were used. The sum of states "5+6"("7+8") gives the positive (negative) tensorially polarized beam without vector polarization admixture. The sum of "5+7"("6+8") gives the positive (negative) vectorially polarized beam without tensorial admixture. The combinations "5+8" and "6+7" give the unpolarized beam. The vector polarization was normal to the plane containing the mean beam orbit of the accelerator. The beam polarization was measured periodically during the experiment with the SATURNE-II low-energy polarimeter (see Table III).

The vector and tensor deuteron polarizations measured near the source are also the polarizations of the beam at the target within very good accuracy, since no depolarizing resonances exist during acceleration in the kinematical region considered. This has been carefully studied before [15] and systematically checked during the numerous experiments carried on in SATURNE with the polarized deuteron beam (see for example [16]).

The average beam polarizations were $P_{ZZ}=0.902\pm0.015$, $P_Z=0.311\pm0.008$, and $|P_Z^+|=|P_Z^-|$ $(|P_{ZZ}^+|=|P_{ZZ}^-|)$, ($P_{ZZ}^{\pm}$ and $P_Z^{\pm}$ are the tensor and vector polarizations where Z is related to the polarized deuteron source coordinate system [17]).

The beam intensity was typically $I\simeq10^6$ deuterons per spill. It was monitored by three independent monitors.

TABLE III. Results of the beam polarization measurements. The measurements were performed periodically (each ~2 days).

Number of the measurement	P_{zz}	P_z
1	0.9047 ± 0.081	-0.3506 ± 0.039
2	0.8978 ± 0.041	-0.3238 ± 0.023
3	0.8940 ± 0.022	-0.3190 ± 0.012
4	0.9298 ± 0.036	-0.2848 ± 0.018
5	0.9004 ± 0.033	-0.3044 ± 0.017

(1) A relative monitor consisted of two independent detector arms each consisting of a telescope of three small scintillation counters. Particles knocked out from a 250-μm Ta foil placed in the beam 5 m upstream the LH target were detected by each arm independently.

(2) Secondary emission chamber. The beam traversed a metal foil, and the emitted free electrons were collected on an anode. The number of secondary electrons is proportional to the beam intensity.

(3) A scintillation counter (SBEAM), operating at lowered voltage, which was placed in the direct incoming beam just before the hole in the Tethys yoke. The thickness of scintillator was about 0.5 cm.

These methods gave the relative beam intensity, and it was checked that they were consistent with each other. In data analysis the relative beam intensity measured by SBEAM was used because the highest counting rate of this monitor provided a minimal statistical error that was important in the polarization measurements. It was found that its counting rate was proportional to the beam intensity, which was checked periodically by the measurement of the activation of a thin carbon target inserted in the beam for 10 min. The ratios of the counting rates of this monitor to the other ones were verified to be constant for all bursts used in the data analysis.

III. MEASURED QUANTITIES

The main goal of the present experiment was the measurement of the analyzing powers A_{yy} and A_y for reactions (1)–(3). Following the Madison convention [17], a cartesian coordinate system was used with the z axis along the incident beam, the y axis normal to the scattering plane (and parallel to the direction of the incident deuteron spin quantization axis), the x axis defined a right-handed coordinate system. The cross section of the dp inelastic scattering can then be written as

$$\sigma^{\pm}(\theta_\pi,t)=\sigma^0(\theta_\pi,t)\left[1+\frac{3}{2}P_Z^{\pm}A_y(\theta_\pi,t)+\frac{1}{2}P_{ZZ}^{\pm}A_{yy}(\theta_\pi,t)\right], \quad (7)$$

where σ^0 and $\sigma^{\pm}$ are the cross sections for unpolarized and polarized beam, "0," "+," "−" denote the corresponding beam polarization, $A_y(\theta_\pi,t)$ and $A_{yy}(\theta_\pi,t)$ are the vector

and tensor analyzing powers of the reaction, θ_π is the horizontal pion emission angle, and t is the deuteron four-momentum transfer squared.

It is easy to solve Eq. (7) using the combination of the polarization states with tensorially polarized beam without vector polarization admixture and the vectorially polarized beam without tensor polarization admixture if $|P_Z^+|=|P_Z^-|$ ($|P_{ZZ}^+|=|P_{ZZ}^-|$):

$$A_{yy}(\theta_\pi,t)=\frac{2}{P_{ZZ}}\frac{\sigma^+{}_t-\sigma^-{}_t}{\sigma^+{}_t+\sigma^-{}_t}, \tag{8}$$

$$A_y(\theta_\pi,t)=\frac{2}{3P_Z}\frac{\sigma^+{}_v-\sigma^-{}_v}{\sigma^+{}_v+\sigma^-{}_v}, \tag{9}$$

where $\sigma^{\pm}{}_{t,v}$ are the cross sections for the tensorially (vectorially) polarized beam.

In this experiment the tensor A_{yy} and vector A_y analyzing powers were calculated for each selected reaction by the following way:

$$A_{yy}(\theta_\pi,t)=\frac{2}{P_{ZZ}}\frac{N_5+N_6-N_7-N_8}{N_5+N_6+N_7+N_8}, \tag{10}$$

$$A_y(\theta_\pi,t)=\frac{2}{3P_Z}\frac{N_5-N_6+N_7-N_8}{N_5+N_6+N_7+N_8}, \tag{11}$$

$$A_0(\theta_\pi,t)=\frac{N_5-N_6-N_7+N_8}{N_5+N_6+N_7+N_8}. \tag{12}$$

Here N_5, N_6, N_7, and N_8 are the numbers of events detected at each beam polarization state normalized to the corresponding beam intensities.

The last equation represents the false asymmetry. This asymmetry was checked for all reaction channels and was consistent with zero in all cases, proving the polarization observables to be under full control.

IV. MEASUREMENTS

The measurements were done at the deuteron beam momentum 3.73 GeV/c with three different settings of the SPES4 and Tethys magnetic fields, to assure a complete coverage of the Roper resonance mass region (Fig. 4). The central momentum settings of the SPES4 spectrometer were 2.85 GeV/c, 2.94 GeV/c, and 3.04 GeV/c. The corresponding regions of the four-momentum transfer squared t were for 2.85 GeV/c $-0.28\leqslant t\leqslant -0.14$ $(\mathrm{GeV}/c)^2$, for 2.94 GeV/c $-0.22\leqslant t\leqslant -0.1$ $(\mathrm{GeV}/c)^2$, for 3.04 GeV/c $-0.17\leqslant t\leqslant -0.07$ $(\mathrm{GeV}/c)^2$. The Tethys and SPES4 magnetic fields were varied proportionally, assuring identical trajectories of the deuterons accepted by SPES4. The field strengths were monitored by use of nuclear magnetic resonance probe with accuracy better than 1 Gauss.

The coincidences of signals from SPES4 (see above) and the scintillation hodoscopes of the FS were used for triggering, SPES4 (FS+LS).

For each setting background measurements with the empty target were performed periodically. The ''full''-to-''empty'' event ratio, after all selection criteria were applied, amounted to $\simeq 20$.

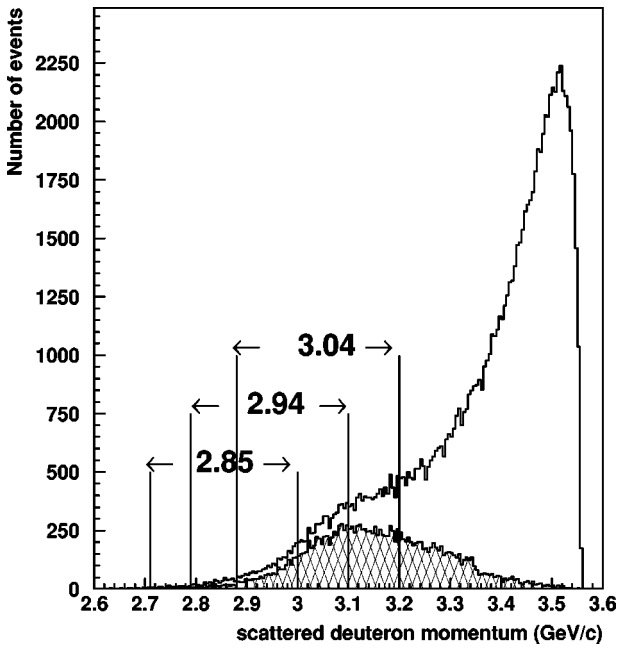

FIG. 4. Momentum spectrum of the scattered deuterons. The distribution is generated according to [22]. Regions, covered by the setup acceptance corresponding to the different spectrometer settings, with the central momenta of scattered deuterons of 2.85 GeV/c, 2.94 GeV/c, and 3.04 GeV/c are indicated. Dashed region corresponds to the Roper resonance excitation.

The summary of the main characteristics of the setup and the data taking is given in Table I.

V. DATA ANALYSIS AND RESULTS

A. Identification of the reaction channels

The detected events originated mainly from the inelastic $p(d,d')N\pi(\pi)$ reactions, elastic backward (in c.m.s.) $p(d,p)d$ scattering, and the breakup $p(d,p)pX$ reaction [18], as seen in Fig. 5. The protons from these processes that were in the momentum range of $\pm 4\%$ from the central momentum of SPES4 settings, were registered by SPES4 but were identified by (time of flight, momentum) correlations inambiguously (see Fig. 5). Background due to quasielastic NN scattering was suppressed at the trigger level already by requirement of coincidences between FS and the focusing spectrometer SPES4. This kind of the background contributes in the random rates only.

The elastic process was unambiguously identified by detecting the recoil proton in SPES4 ($p_p\simeq 2.93$ GeV/c) in coincidence with the scattered deuteron in the FS ($p_d \simeq 0.8$ GeV/c). It provided useful information for the calibration of the setup [13,14]. The data on the $p(d,p)d$ tensor analyzing power, obtained in the present experiment and published in [18], agree well with the existing world data [19,20].

For the inelastic process $p(d,d')X$, $X=N\pi(\pi)$, the scattered deuterons were detected by SPES4, while the charged

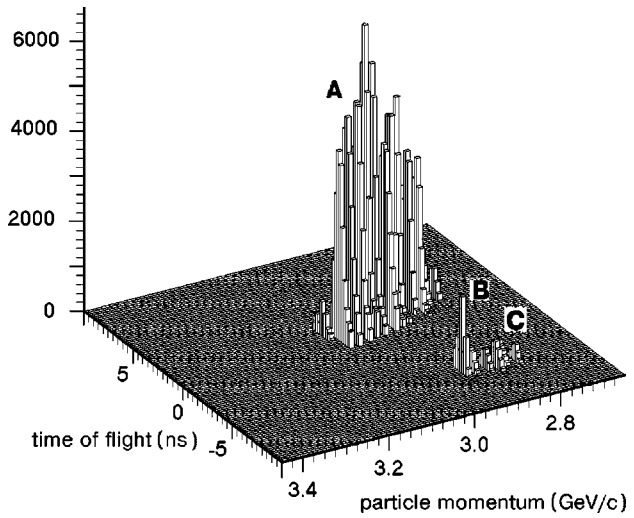

FIG. 5. Experimental plot of ''momentum in SPES4'' (GeV/c)—''time of flight in SPES4'' (ns). (A): Deuterons in the SPES4 from inelastic $p(d,d')$ (the big ''mountain''), (B) protons from $p(d,p)d$ (the small peak), (C) protons from the $p(d,p)pX$ reactions (the tail of the small peak). These regions are well separated.

products of the decay of the intermediate system X were registered by the forward spectrometer.

The calculated missing mass was used for the identification of the reaction channels,

$$m_x^2=(k_d+k_{target}-k_d'-k_{ch})^2,$$

where k_d, k_d', $k_{target}=(m_{target},0,0,0)$, $k_{ch}=(E_{ch},\vec{p}_{ch})$, are respectively the four-momenta of the incident deuteron, scattered deuteron, target proton, and charged particle detected in the FS (π^+ or proton). The particles in the FS were identified by time-of-flight (TOF) and energy loss (ADC, amplitude-to-digit converter units) measurements. The two-dimensional plots of the TOF versus the energy loss, TOF versus the particle momentum, and ADC versus the particle momentum were constructed for each counter of the FS hodoscope and the selection criteria were chosen separately for each counter and for each setting (see an example of such distributions in Fig. 6). Note that the probability to misidentify π^+ as protons or proton as π^+ increases with increasing particle momentum. Particles with momenta below 0.7 GeV/c can be identified unambiguously. For particles with momenta above 0.7 GeV/c the possibility of different identification was considered separately by the missing mass calculations.

We analyzed events in which one charged particle was detected by the FS and the scattered deuteron by the SPES4. A specific feature of the experiment was that the secondary particles from different reactions populate different angular and momentum regions. In Figs. 7(b)–7(f) the regions of kinematical variables accepted by the setup for all considered reactions are presented. These regions were mapped with a Monte Carlo simulation using phase space distributions of the particles, with cuts implied by the setup boundaries and the trigger conditions. The sizes of the FS holes were enlarged in the data analysis (and in the simulation) in order to eliminate random triggers and were set at 18×13 cm^2 in the chambers and 25×30 cm^2 in the hodoscope.

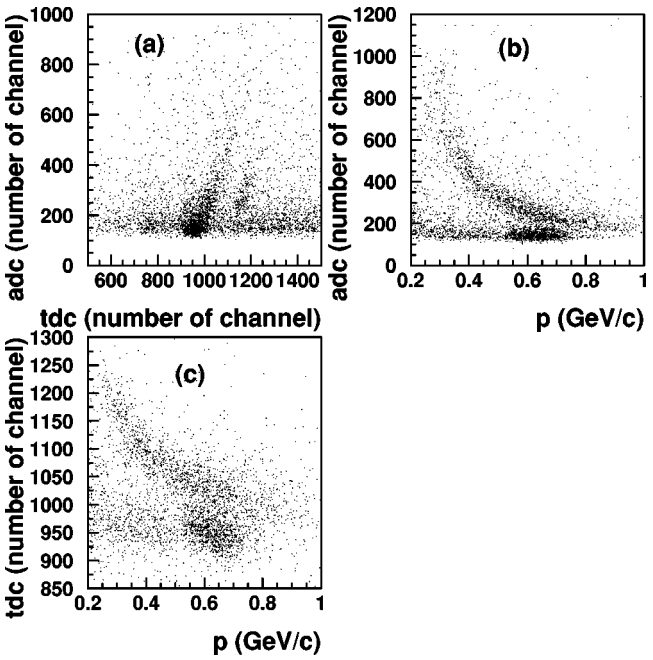

FIG. 6. Plots for the particle identification for the FS hodoscope counter number 3 at the SPES4 setting 2.94 GeV/c. (a) Time of flight (TOF) versus amplitude (ADC), both in arbitrary units. (b) ADC versus the charged particle momentum. (c) TOF (in time-to-digit converter units) versus the charged particle momentum.

The choice of the experimental cuts for the channel selection was verified by the Monte Carlo calculations.

If the particle registered in the FS was identified as a positive pion, the missing mass distribution should have a peak close to the neutron mass corresponding to $dp\rightarrow dn\pi^+$ reaction and a broader structure at higher mass corresponding to the reaction $dp\rightarrow dN\pi^+\pi$.

If the particle registered in the FS was identified as a proton then the missing mass distribution should have a peak close to the π^0 mass corresponding to the $dp\rightarrow dp\pi^0$ reaction and a broader distribution at higher mass corresponding to $dp\rightarrow dp\pi\pi$ reaction.

The π^- were not considered due to low acceptance for π^- registration by the FS.

The results of A_{yy} and A_y measurements are presented in Table IV. The errors shown there are only statistical.

1. One-pion production channels

$dp\rightarrow dn\pi^+$ reaction. Figure 8 shows the selection of events from the $dp\rightarrow dn\pi^+$ reaction. Positive pions from this reaction were detected by the FS. For each setting of the SPES4 spectrometer the region of the corresponding four-momentum transfer squared t was divided into three equal parts (bins). In Fig. 9 the missing mass squared spectra corresponding to the unobserved neutron from the $dn\pi^+$ final state are shown for each $|t|$ bin for both tensor polarization states. The corresponding spectra taken with ''empty target'' measurements were subtracted. The background from par-

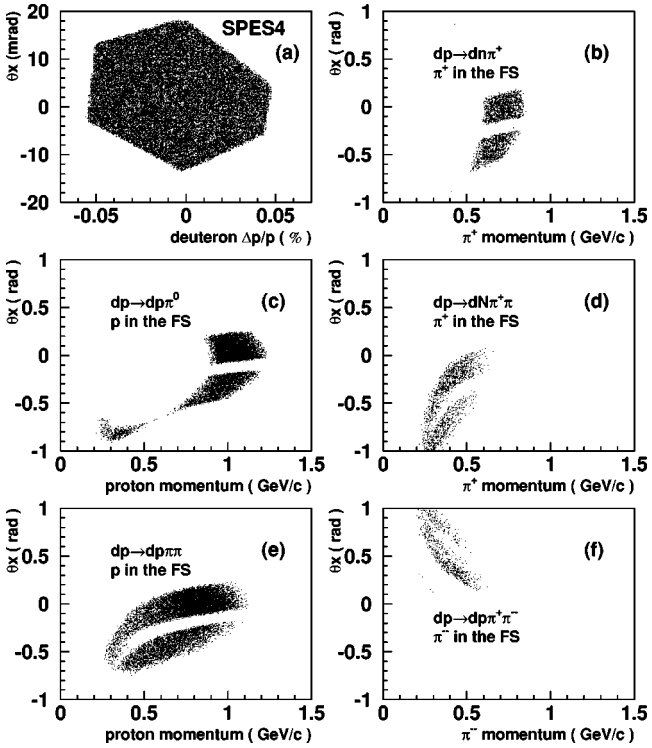

FIG. 7. Acceptance of the setup for different reaction channels, calculated using GEANT package. d' is accepted by the SPES4. Events were generated by phase space simulation code GENBOD. (a) Momentum versus the horizontal emission angle of deuterons accepted by the SPES4. (b)–(f) Momentum versus the horizontal emission angle of the charged particle from $dp\rightarrow dN\pi(\pi)$ reactions accepted by the FS.

ticle misidentification (very small) was fitted by a polynomial and subtracted. Similar spectra were obtained for all three settings of SPES4.

In Figs. 10(a)–10(c) the tensor analyzing power A_{yy}, vector analyzing power A_y, and the false asymmetry A_0 are presented for this reaction as a function of the mean $|t|$ value of the bin. The regions covered by the SPES4 settings, $(\Delta p_d/p_d=\pm 4\%)$ overlapped (Fig. 4), so it is possible to compare the values of the polarization observables measured at different settings of the spectrometer. From Fig. 10(a) one can see that these measurements are consistent, and then the average values of A_{yy} are taken for each $|t|$, Fig. 10(d). A similar method was used for all other reaction channels.

$dp\rightarrow dp\pi^0$ reaction. In Fig. 11 the selection of events from the $dp\rightarrow dp\pi^0$ channel is shown for the SPES4 spectrometer setting 2.94 GeV/c when protons were detected in the FS. Similar plots were obtained for settings 2.85 GeV/c and 3.04 GeV/c. In Fig. 11(a) the spot near zero missing mass squared corresponds to $dp\rightarrow dp\pi^0$ reaction; the other events are from $dp\rightarrow dp\pi\pi$ and from misidentified positive pions from the reaction $dp\rightarrow dn\pi^+$. In Fig. 11(b) the two-dimensional distribution of the proton horizontal emission angle (θ_x) and momentum is shown. The rectangle in the lower left corner indicates the selection criteria for the events from $dp\rightarrow dp\pi^0$ reaction. This has to be put together with the calculated range of the accepted proton momenta and angles shown in Fig. 7(c). The latter consists of two parts, corresponding to protons with $p_p<0.5$ and $p_p>0.7$ GeV/c, respectively. Only protons with momenta $p_p<0.5$ GeV/c could be identified reliably in the experiment. For this reaction it was impossible to distinguish protons with momenta $p_p>0.7$ GeV/c from the strong background of misidentified particles; consequently these events were rejected. The rectangle in the lower left corner indicates the selection criteria for the events from $dp\rightarrow dp\pi^0$ reaction. In the bottom part of Fig. 11 the distributions of the missing mass squared are shown. Figure 11(c) represents the one without application of the selection criteria. Figure 11(d) shows the one for protons with $\theta_x<-0.7$ rad and $p_p<0.5$ GeV/c. A clear signal for π^0 events was obtained for this part of the proton spectra.

In Figs. 10(d)–10(f) the tensor analyzing power A_{yy}, vector analyzing power A_y, and false asymmetry A_0 are presented. Because of the lack of statistics for this channel, only the mean value of $|t|$ for each setting is taken.

A_{yy} angular and t dependence for the one-pion channels. In general the amplitude for the $dp\rightarrow dN\pi$ reaction depends on the momenta and angles of all outgoing particles, but under the kinematical conditions of this experiment, when the scattered deuterons are detected at angles close to 0° and M_{eff} is directly related with t, the tensor analyzing power A_{yy} is a function of two independent variables only, the horizontal pion emission angle θ_π and t.

$A_{yy}(\theta_\pi,t)$ is presented in Table IV as a function of both variables θ_π and t. The A_{yy} dependencies on t and θ_π, integrated over the accepted values of the other variable are presented in Figs. 10(d)–10(h).

Events from the reactions $dp\rightarrow dn\pi^+$ and $dp\rightarrow dp\pi^0$ detected in the SPES4-π spectrometer populate different regions of the horizontal pion emission angles θ_π (Fig. 12). The accepted angular region for $dp\rightarrow dp\pi^0$ is narrow. On the contrary for the $dp\rightarrow dn\pi^+$ channel it is rather broad and it was divided into three equal parts (bins). The mean value of θ_π over the bin was taken. In Fig. 10(g) the dependence of A_{yy} upon θ_π (for positive pion from $dp\rightarrow dn\pi^+$ and for neutral pion from $dp\rightarrow dp\pi^0$) reactions is presented. Three points for $dp\rightarrow dn\pi^+$ and one for $dp\rightarrow dp\pi^0$ are shown. All possible values of $|t|$ are included, which is equivalent to integration over the whole $|t|$ range. It is seen in this figure that the A_{yy} is an even smooth function of θ_π, A_{yy} values being almost the same for the points with the similar absolute values of θ_π.

If we plot A_{yy} as a function of $|t|$ only (which corresponds to the integration over the horizontal pion emission angles allowed by the setup, i.e., $-36°<\theta_{\pi^+}<6°$ for $dn\pi^+$ and $6°<\theta_{\pi^0}<36°$ for $dp\pi^0$ final states) the values of A_{yy} for the discussed $dp\rightarrow dN\pi$ channels with the same $|t|$ values are essentially different [Fig. 10(d)]. This is due to the different θ_π range selected in both cases.

A_y angular and t dependence for the one-pion channels. Similar to A_{yy}, the one pion asymmetry, A_y, for $dp\rightarrow dN\pi$ shows a strong angular dependence [Fig. 10(h)]. It is an odd function of the angle, consistent with zero at zero-pion emission angles. The A_y angular dependence seems to be understood qualitatively if one takes into account that in collinear kinematics (d' is detected at about zero angle) the

TABLE IV. Spin-dependent observables A_{yy} and A_y.

t $(\mathrm{GeV}/c)^2$	$\langle\lvert t\rvert\rangle$ $(\mathrm{GeV}/c)^2$	θ_π (deg)	A_{yy}	A_y
		$dp\to dn\pi^+$, π^+ is detected in the FS		
	0.22 ± 0.02	$-36^\circ\leqslant\theta_{\pi^+}\leqslant6^\circ$	0.516 ± 0.081	-0.004 ± 0.078
	0.19 ± 0.01	$-36^\circ\leqslant\theta_{\pi^+}\leqslant6^\circ$	0.327 ± 0.046	0.107 ± 0.044
	0.15 ± 0.01	$-36^\circ\leqslant\theta_{\pi^+}\leqslant6^\circ$	0.294 ± 0.032	0.091 ± 0.031
	0.12 ± 0.01	$-36^\circ\leqslant\theta_{\pi^+}\leqslant6^\circ$	0.254 ± 0.037	0.196 ± 0.036
	0.08 ± 0.03	$-36^\circ\leqslant\theta_{\pi^+}\leqslant6^\circ$	0.181 ± 0.066	0.247 ± 0.064
$-0.28\leqslant t\leqslant-0.14$	0.19 ± 0.05	$0^\circ\leqslant\theta_{\pi^+}\leqslant8^\circ$	0.349 ± 0.062	-0.011 ± 0.06
$-0.28\leqslant t\leqslant-0.14$	0.19 ± 0.05	$-10^\circ\leqslant\theta_{\pi^+}\leqslant0^\circ$	0.262 ± 0.068	0.051 ± 0.06
$-0.28\leqslant t\leqslant-0.14$	0.19 ± 0.05	$-38^\circ\leqslant\theta_{\pi^+}\leqslant-18^\circ$	0.525 ± 0.083	0.161 ± 0.08
$-0.22\leqslant t\leqslant-0.1$	0.15 ± 0.05	$0^\circ\leqslant\theta_{\pi^+}\leqslant8^\circ$	0.307 ± 0.056	-0.033 ± 0.055
$-0.22\leqslant t\leqslant-0.1$	0.15 ± 0.05	$-10^\circ\leqslant\theta_{\pi^+}\leqslant0^\circ$	0.259 ± 0.048	0.130 ± 0.045
$-0.22\leqslant t\leqslant-0.1$	0.15 ± 0.05	$-38^\circ\leqslant\theta_{\pi^+}\leqslant-18^\circ$	0.411 ± 0.065	0.234 ± 0.064
$-0.17\leqslant t\leqslant-0.07$	0.12 ± 0.05	$0^\circ\leqslant\theta_{\pi^+}\leqslant8^\circ$	0.268 ± 0.079	-0.041 ± 0.072
$-0.17\leqslant t\leqslant-0.07$	0.12 ± 0.05	$-10^\circ\leqslant\theta_{\pi^+}\leqslant0^\circ$	0.123 ± 0.052	0.197 ± 0.051
$-0.17\leqslant t\leqslant-0.07$	0.12 ± 0.05	$-38^\circ\leqslant\theta_{\pi^+}\leqslant-18^\circ$	0.425 ± 0.098	0.298 ± 0.091
		$dp\to dp\pi^0$, p is detected in the FS		
$-0.28\leqslant t\leqslant-0.14$	0.19 ± 0.02	$6^\circ\leqslant\theta_{\pi^0}\leqslant36^\circ$	0.428 ± 0.120	-0.204 ± 0.110
$-0.22\leqslant t\leqslant-0.1$	0.15 ± 0.02	$6^\circ\leqslant\theta_{\pi^0}\leqslant36^\circ$	0.521 ± 0.076	-0.115 ± 0.071
$-0.17\leqslant t\leqslant-0.07$	0.12 ± 0.02	$6^\circ\leqslant\theta_{\pi^0}\leqslant36^\circ$	0.374 ± 0.065	-0.144 ± 0.061
		$dp\to dN\pi^+\pi$, π^+ is detected in the FS		
	0.22 ± 0.01	$-56^\circ\leqslant\theta_{\pi^+}\leqslant0^\circ$	0.314 ± 0.089	0.031 ± 0.086
	0.19 ± 0.01	$-56^\circ\leqslant\theta_{\pi^+}\leqslant0^\circ$	0.438 ± 0.062	0.005 ± 0.060
	0.15 ± 0.01	$-56^\circ\leqslant\theta_{\pi^+}\leqslant0^\circ$	0.382 ± 0.062	0.048 ± 0.046
	0.12 ± 0.01	$-56^\circ\leqslant\theta_{\pi^+}\leqslant0^\circ$	0.259 ± 0.062	0.053 ± 0.060
	0.08 ± 0.03	$-56^\circ\leqslant\theta_{\pi^+}\leqslant0^\circ$	0.21 ± 0.17	-0.10 ± 0.16
		$dp\to dp\pi\pi$, p is detected in the FS		
	0.22 ± 0.01	$-60^\circ\leqslant\theta_{\pi(-,+,0)}\leqslant60^\circ$	0.351 ± 0.054	0.026 ± 0.048
	0.19 ± 0.01	$-60^\circ\leqslant\theta_{\pi(-,+,0)}\leqslant60^\circ$	0.373 ± 0.038	0.046 ± 0.036
	0.15 ± 0.01	$-60^\circ\leqslant\theta_{\pi(-,+,0)}\leqslant60^\circ$	0.317 ± 0.028	0.036 ± 0.026
	0.12 ± 0.01	$-60^\circ\leqslant\theta_{\pi(-,+,0)}\leqslant60^\circ$	0.250 ± 0.028	0.036 ± 0.027
	0.08 ± 0.03	$-60^\circ\leqslant\theta_{\pi(-,+,0)}\leqslant60^\circ$	0.193 ± 0.050	0.005 ± 0.048

reaction plane is determined by the momentum vector of a secondary particle and the incoming beam direction; therefore when they are almost collinear ($\theta_\pi\sim0$), the reaction plane becomes undefined.

A_y as a function of $|t|$, integrated over the pion emission angles allowed by the setup, has different signs for $dp\to dn\pi^+$ and $dp\to dp\pi^0$ channels at the same $|t|$ values [Figs. 10(b) and 10(e)]. This is a consequence of the different θ_π range selected.

The dependence of A_y on θ_π and t is presented in Table IV, for each bin of θ_π the mean value of $|t|$ for the whole setting is given.

2. Two-pion production channels

Channel selection. In this experiment the events from the reaction channels with two pions in the final state are selected when either π^+ or protons were detected in the FS.

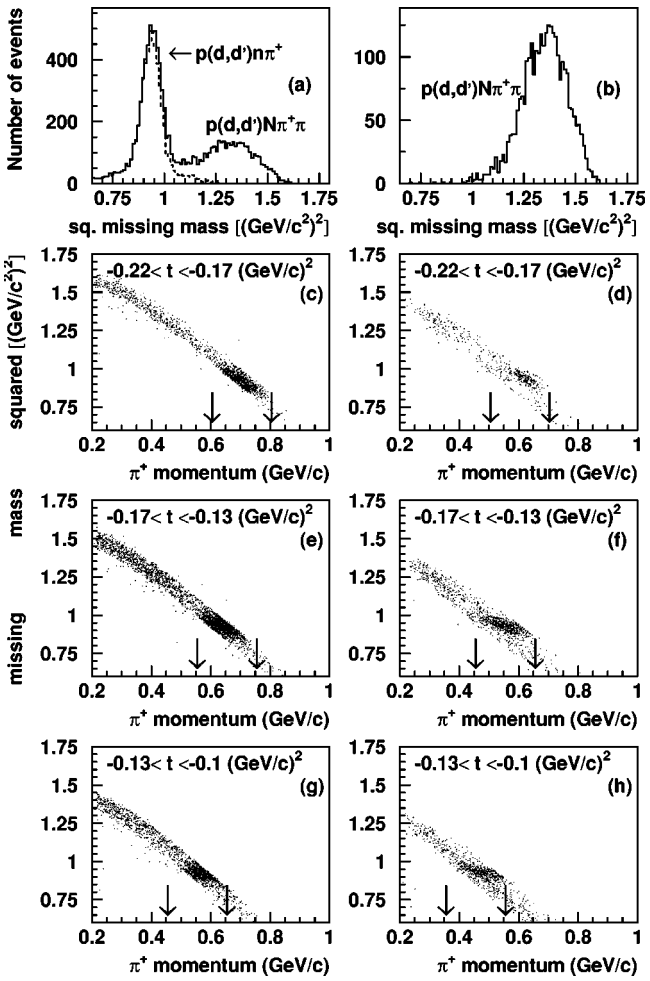

FIG. 8. Experimental missing mass squared distributions for the $dp \rightarrow dN\pi^+(\pi)$ channels when π^+ is detected by the FS at the central momentum of SPES4 equal to 2.94 GeV/c. (a) Missing mass squared distribution for all selected events from $dp \rightarrow dN\pi^+(\pi)$. Dotted line corresponds to the events from $dn\pi^+$. (b) Missing mass squared distribution for events from $dN\pi^+\pi$. Figures (c)–(g) represent the missing mass squared versus momentum of π^+ distributions for different intervals of t. Figures (c), (e), and (g) represent the distributions for the left part of the X chambers; figures (d), (f), and (h) represent the distributions for the right one. The cuts on the momentum of π^+ for the selection of events from $dn\pi^+$ were chosen for each interval of t and for each part of the X chambers separately [solid arrows in the Figs. (c)–(h)].

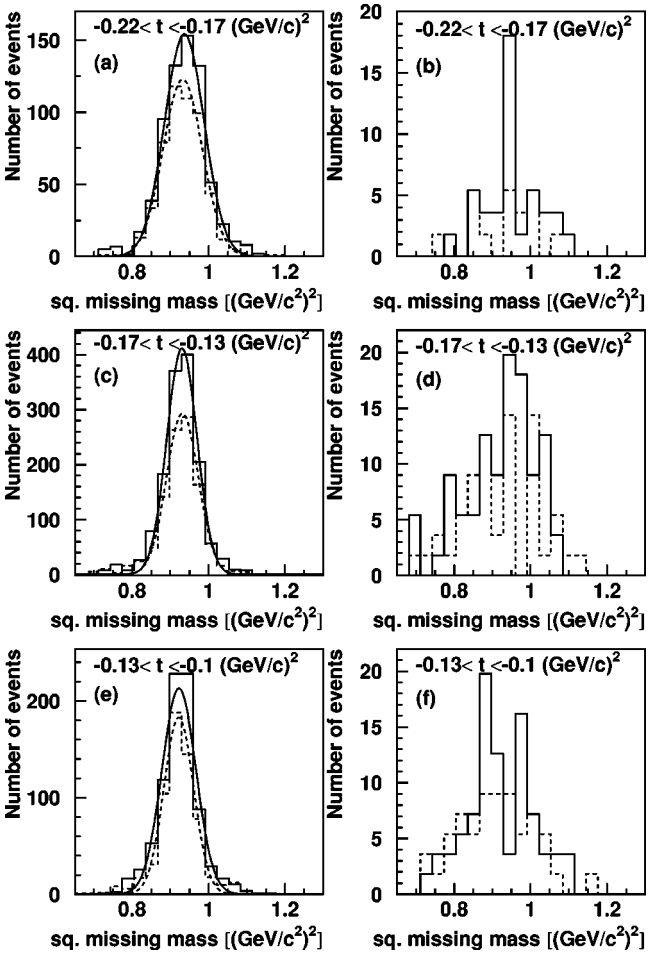

FIG. 9. Experimental missing mass squared distributions for the $dp \rightarrow dn\pi^+$ channel when π^+ is detected by the FS at the central momentum of SPES4 equal to 2.94 GeV/c. Solid line: the positive tensorial polarization of the beam; dashed line: the negative tensorial polarization.

The case when π^- were detected by the FS was not considered due to low acceptance for π^- registration [Fig. 7(f)].

In Fig. 8(b) the missing mass squared spectrum for events from $dp \rightarrow dN\pi^+\pi^-$ with π^+ detected in the FS is shown. The selection criteria are complementary to those used for $dp \rightarrow dn\pi^+$ with pion momentum less than 0.5 GeV/c and angle $\theta_\pi < 0$ (see Figs. 4 and 7).

A_{yy} and A_y t dependence for the two-pions channels. In Fig. 13 the tensor analyzing power A_{yy}, vector analyzing power A_y, and the false asymmetry A_0 are presented for the two-pion production channels as functions of t. The data for A_{yy} were obtained in both ways: when π^+ were detected in the FS or when protons were detected in the FS; the results coincide. As only one charged particle was detected in addition to the deuteron, the measured observables were integrated over all possible angles (and momenta) of the nonregistered particles. The values of A_y and A_{yy} are very similar in the case of detection of a pion or of a proton for the same momentum transfer, moreover the vector analyzing power A_y for these channels is close to zero: see Figs. 13(b) and 13(e). This can be explained in the following way: both when π^+ or a proton is detected, there is no defined reaction plane (in contrast with $dp \rightarrow dN\pi$ reactions), and therefore there is no reason to expect a dependence of A_{yy} and A_y on θ_π; moreover the vector analyzing power A_y for these channels is close to zero: see Figs. 13(b) and 13(e).

3. Comparison of t-dependence of A_{yy} for one- and two-pion production channels

The difference between the tensor analyzing power A_{yy} for the reaction $dp \rightarrow dn\pi^+$ and for the channels with two pions in the final state is not significant (Fig. 14 and Table IV). They actually differ only at the point with the maximum $|t|$, $t = -0.225$ (GeV/c)^2. As discussed before it was expected that two-pion final states correspond to the pure N^*

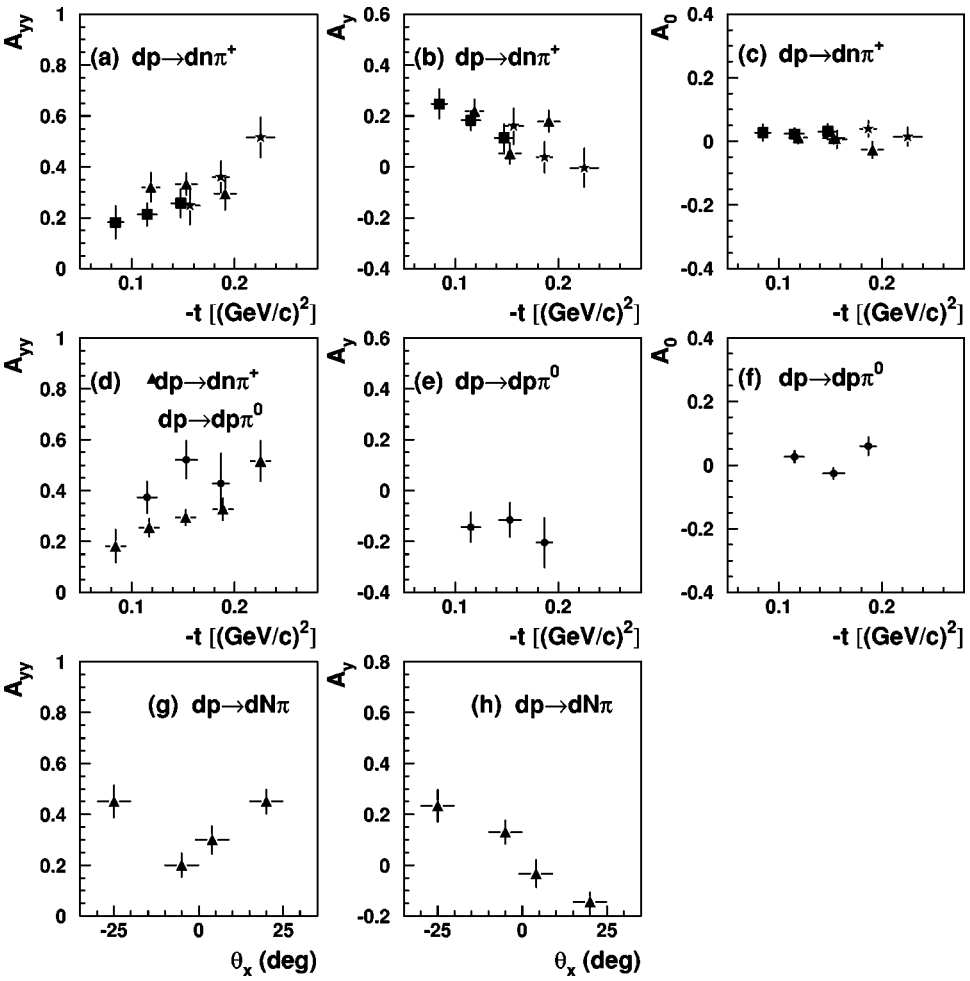

FIG. 10. Data for the spin-dependent observables A_{yy} and A_y versus t and θ_π for the one-pion production channels. Squares: the setting corresponding to the central momentum of SPES4 3.04 GeV/c; triangles: 2.94 GeV/c; stars: 2.85 GeV/c; (a) Tensor analyzing power A_{yy} versus $|t|$, for each setting separately. (b) Vector analyzing power A_y versus $|t|$, for each setting separately. (c) False asymmetry A_0 versus $|t|$, for each setting separately. (d) Mean values of A_{yy} for $dn\pi^+$, π^+ detected by the FS (triangles); A_{yy} for $dp\pi^0$, p detected by the FS (filled circles). (e) Vector analyzing power A_y for $dp\pi^0$ channel. (f) False asymmetry A_0 for the $dp\pi^0$ channel. (g) Mean values of A_{yy} for $dn\pi^+$ (triangles) and A_{yy} for $dp\pi^0$ (filled circles) versus the horizontal emission angle of the pion in the lab system. (h) Mean values of A_y for $dn\pi^+$ (triangles) and A_y for $dp\pi^0$ (filled circles) versus the horizontal emission angle of the pion in the lab system.

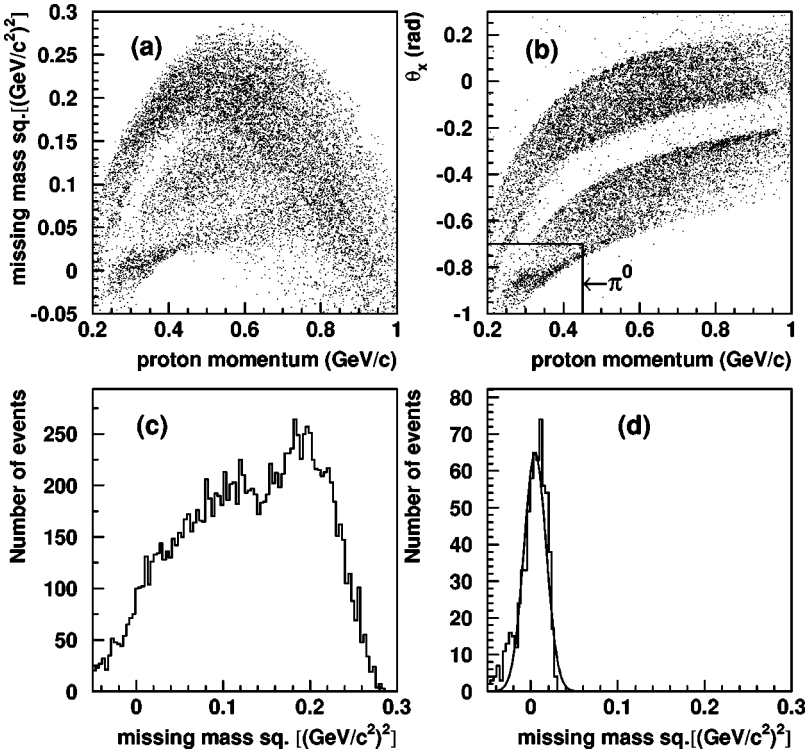

FIG. 11. Experimental distributions for the $dp\rightarrow dp\pi(\pi)$ reaction, when the protons were registered in the FS at the central momentum of SPES4 equal to 2.94 GeV/c. (a) Missing mass squared versus the proton momentum. (b) Horizontal emission angle versus the proton momentum. (c) Missing mass squared for the $dp\rightarrow dp\pi(\pi)$ reaction (without cuts). (d) Missing mass squared of π^0.

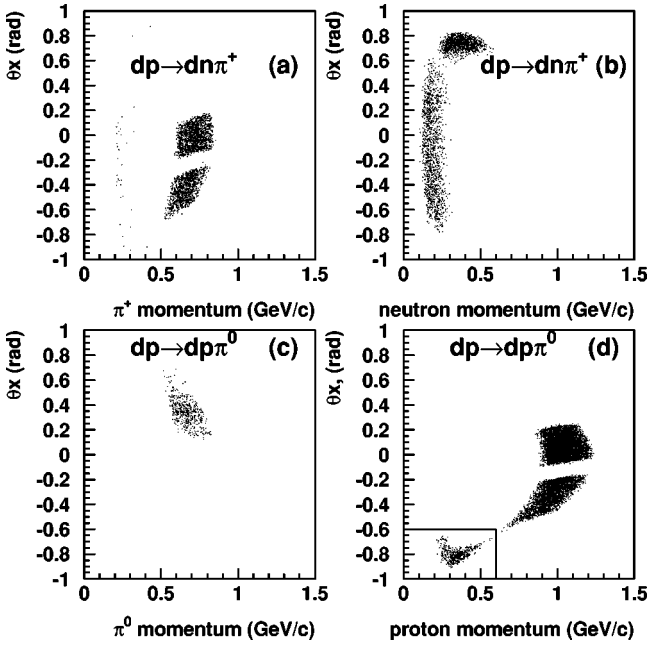

FIG. 12. Monte Carlo simulation of the reaction channels: $dp \rightarrow dp\pi^0$; $dp \rightarrow dn\pi^+$: momentum versus the horizontal emission angle of a secondary particle. The events were generated by the phase space simulation code GENBOD. The scattered deuterons are accepted by the SPES4.

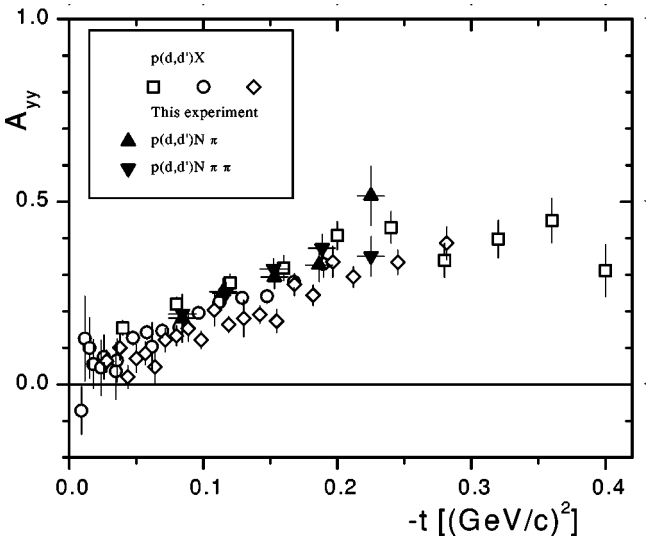

FIG. 14. Comparison of the tensor analyzing power A_{yy} for $p(d,d')X$ (world data [6]) with the results of this experiment for the reactions $dp \rightarrow dn\pi^+$ and $dp \rightarrow dp\pi\pi$. World data: the squares, circles, and diamonds correspond to $p_d = 9$ GeV/c, $p_d = 5.5$ GeV/c, $p_d = 4.5$ GeV/c.

signal, for one-pion final states both Δ and N^* resonances give a contribution. In the low $|t|$ region the Δ excitation in the projectile dominates in inclusive $dp \rightarrow dX$ [5], but according to Monte Carlo simulation of our setup with the

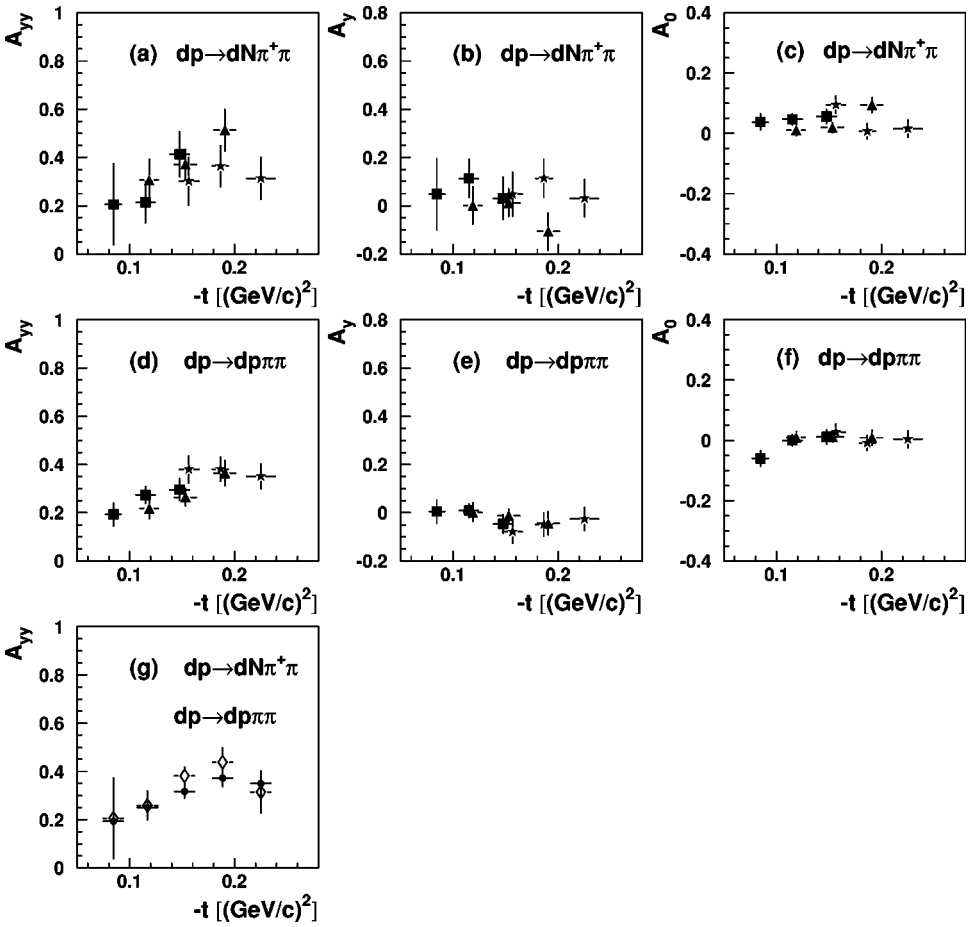

FIG. 13. Data on the spin-dependent observables A_{yy}, A_y, and A_0 for the two-pion final states. In all the panels, squares correspond to the setting with the central momentum of SPES4 3.04 GeV/c; triangles: 2.94 GeV/c; stars: 2.85 GeV/c; (a)–(c) for $dN\pi^+\pi$, when π^+ is detected by the FS: (a) Tensor analyzing power A_{yy}. (b) Vector analyzing power A_y. (c) False asymmetry A_0. (d)–(f) For $dp\pi\pi$, when p is detected by the FS. (d) Tensor analyzing power A_{yy}. (e) Vector analyzing power A_y. (f) False asymmetry A_0. (g) Mean values of A_{yy} for $dN\pi^+\pi$ (empty diamonds), π^+ detected by FS; A_{yy} for $dp\pi\pi$ (filled circles), protons detected by the FS.

matrix element of [22] (Fig. 4) it is expected that contribution of the $\Delta(1232)$ resonance excitation in the projectile is suppressed in our experiment and does not exceed one-fourth of the N^* contribution even at the highest setting of SPES4, 3.04 GeV/c. The simplest possible interpretation of the absence of the difference between tensor analyzing power for one- and two-pion production channels is that the exclusive reaction in the kinematics of this experiment is fully dominated by the Roper. This interpretation is based on the [22] consideration of the $p(d,d')X$ reaction.

In Fig. 14 the data for these reaction channels are compared with the existing world data from the inclusive $p(d,d')X$ scattering. The inclusive data on A_{yy} demonstrate an approximate scaling in $|t|$, but the points corresponding to the exclusive measurements are higher (compare triangles with diamonds in Fig. 14) than the inclusive ones when taken at the closest beam momentum ($p_d = 4.5$ GeV/c). It may be explained by hypothesizing that the integration over the full phase space of the missing mass in (d,d') allows some other contributions that lowers A_{yy} somewhat.

VI. CONCLUSIONS

Tensor and vector analyzing powers for the reactions $dp \rightarrow dn\pi^+$, $dp \rightarrow dp\pi^0$, $dp \rightarrow dN\pi\pi$ were measured in the energy region of the Roper $N(1440)$ resonance excitation as functions of the deuteron four-momentum transfer squared in the t range, $-0.28 \leqslant t \leqslant -0.07$ $(\mathrm{GeV}/c)^2$, of the effective mass of the subsystems $(N\pi)$, $(N\pi\pi)$, $1.33 \leqslant \mathrm{M}_{eff} \leqslant 1.48$ GeV/c^2, and of the pion emission angle. The results are presented in Table IV and in Figs. 10, 13, and 14.

The results of this experiment show two interesting features.

(1) Taken as a function of t, one- and two-pions production channels have the same values of A_{yy} within statistical uncertainty,

(2) Compared to the world data at the nearest beam energy on inclusive $p(d,d')X$, the exclusive A_{yy} data are systematically higher than the inclusive ones.

ACKNOWLEDGMENTS

This work was supported in part by INTAS-RFBR Grant No. 95-1345 and by the Russian Foundation for Fundamental Physics Program Grant No. 122-03. Two participants acknowledge support from the U.S. Department of Energy (V.P., Grant No. DE-FG05-89ER40525) and from the U.S. National Science Foundation (C.F.P., Grant No. 97-04502). We are thankful for the financial support from IN2P3 and IPN. We are grateful to the staff of the Laboratoire National Saturne (Saclay) and Institut de Physique Nucléaire (Orsay) for the hospitality and support during this work. We thank Professor A. A. Vorobyov for stimulating discussions and for support in the FS design and construction. We thank Professor L. S. Azhgirey for fruitful collaborative work and his contribution to the codes used in data analysis. We are thankful to Professor E. Oset and Dr. S. Hirenzaki for the stimulating discussions and providing us with the program code [22] used for event generation in the period of the preparation of this experiment. We are also very grateful to Professor M. P. Rekalo for fruitful discussions.

[1] L. S. Azhgirey *et al.*, Yad. Fiz. **27**, 1027 (1978) [Sov. J. Nucl. Phys. **27**, 544 (1978)]; **30**, 1578 (1979) [**30**, 818 (1979)]; V. G. Ableev *et al.*, *ibid.* **37**, 348 (1983) [*ibid.* **37**, 209 (1983)]; L. S. Azhgirey *et al.*, *ibid.* **48**, 1758 (1988) [*ibid.* **48**, 1058 (1988)].
[2] J. Banaigs *et al.*, Phys. Lett. **45B**, 535 (1973); R. Baldini *et al.*, Nucl. Phys. **A379**, 477 (1982).
[3] Y. Akimov *et al.*, Phys. Rev. Lett. **35**, 763 (1975).
[4] H. P. Morsch *et al.*, Phys. Rev. Lett. **69**, 1336 (1992).
[5] S. Hirenzaki, E. Oset, C. Djalali, and M. Morlet, Phys. Rev. C **61**, 044605 (2000).
[6] L. S. Azhgirey *et al.*, Phys. Lett. B **361**, 21 (1995); L. S. Azhgirey *et al.*, JINR Rapid Commun. **2[88]-98**, 17 (1998).
[7] Data of experiment LNS-250 at SATURNE, Saclay (unpublished).
[8] M. P. Rekalo and E. Tomasi-Gustafsson, Phys. Rev. C **54**, 3125 (1996).
[9] M. P. Rekalo *et al.*, Phys. Rev. C **59**, 1526 (1999).
[10] V. P. Ladygin *et al.*, Eur. Phys. J. A **8**, 409 (2000).
[11] M. Bedjidian *et al.*, Nucl. Instrum. Methods Phys. Res. A **257**, 132 (1987); E. Grorud *et al.*, *ibid.* **188**, 549 (1981).
[12] G. D. Alkhazov, A. V. Kravtsov, and A. N. Prokofiev, PNPI Report No. EP-32-1998 2246, 1998; A. N. Prokofiev *et al.*, Few-Body Syst., Suppl. **10**, 491 (1999).
[13] L. V. Malinina and E. A. Strokovsky, Part. Nuclei Lett. **3**, 86 (2000).
[14] L. S. Azhgirey *et al.*, JINR Rapid Commun. **2[94]-99**, 5 (1999); G. D. Alkhazov, A. V. Kravtsov, and A. N. Prokofiev, PNPI Report No. EP-9-2000, 2000.
[15] J. Arvieux *et al.*, Nucl. Instrum. Methods Phys. Res. A **273**, 48 (1988).
[16] F. T. Baker *et al.*, Phys. Rep. **289**, 235 (1997).
[17] Madison Convention, in *Proceedings of the 3rd International Symposium on Polarization Phenomena in Nuclear Reactions*, Madison, 1970, edited by H. H. Barschall and W. Haeberli (University of Wisconsin, Madison, WI, 1971), pp. XXV–XXIX.
[18] E. A. Strokovsky *et al.*, Few-Body Syst., Suppl. **10**, 495 (1999); G. D. Alkhazov *et al.*, in *Proceedings of the XIV International Seminar on High Energy Physics Problems*, Dubna, 1998, edited by A. M. Baldin and V. V. Burov (JINR, Dubna, 2000), Vol. II, p. 136.
[19] L. S. Azhgirey *et al.*, Phys. Lett. B **391**, 22 (1997); Yad. Fiz. **61**, 494 (1998) [Phys. At. Nucl. **61**, 432 (1998)].
[20] V. Punjabi *et al.*, Phys. Lett. B **350**, 178 (1995).
[21] J. Arvieux *et al.*, Phys. Rev. Lett. **50**, 19 (1983); Nucl. Phys. **A431**, 1613 (1984).
[22] E. Oset, E. Shiino, and H. Toki, Phys. Lett. B **224**, 249 (1989); P. Fernandez de Cordoba and E. Oset, Nucl. Phys. **A544**, 793 (1992); P. Fernandez de Cordoba *et al.*, *ibid.* **A586**, 586 (1995).